Escola de Primavera de Transição e Turbulência
Blumenau 2022

ABCM
13th Spring School on Transition and Turbulence
September 19th-23rd, 2022, Blumenau, SC, Brazil

# EPTT-2022-0082
# NUMERICAL STUDY OF THE INFLUENCE OF THE SCHMIDT NUMBER ON BI-DISPERSE PARTICLE-LADEN GRAVITY CURRENTS

**Guilherme Torres Marques Vidal**
**Rubem Mário Figueiró Vargas**
**Jorge Hugo Silvestrini**
Pontifícia Universidade Católica do Rio Grande do Sul, Escola Politécnica, Av. Ipiranga, 681, Porto Alegre, RS
guilherme_torres@hotmail.com.br, rvargas@pucrs.br, jorgehs@pucrs.br

***Abstract.*** *Density current, or gravity current, is a phenomenon where one fluid flows through another due to a density difference between them. This kind of flow is formed in many natural situations as well as in situations created by humankind, for example, thunderstorm outflows, pyroclastic flows, sandstorms, and others in the manufacturing process, like sheet glass. Because of that, the study of density currents has applications in many different areas like meteorology, atmospheric pollution, entomology, and the industry of gas and oil. This work focus on the numerical study of bi-disperse particle-laden gravity current in the so-called lock-release configuration. The goal is to understand the effect of the Schmidt (Sc) number on the behavior and dynamics of particle-laden density flows and the formation of their deposits. Simulations using direct numerical simulation (DNS) and implicit large eddy simulation (LES) are performed. Three cases are evaluated for the Schmidt number using the LES approach: (i) unitary value for both particle fractions, (ii) Sc=3 and Sc=1 for coarse and fine particle fractions respectively, (iii) and Sc=9 and Sc=3 for coarse and fine particle fractions. Also, a simulation using the DNS approach for unitary value for both particle fractions of Schmidt number is performed as a reference case. All simulations have a Reynolds (Re) number of 5000. To quantify the study some features of the flow are calculated like the position of the current head, suspended mass, and height of deposit profile. Also, the temporal evolution of the energy budget of the simulations is computed. The results of the simulations are compared with previous physical approach experiments available in the bibliography, getting a good agreement. Analyzing the effect of Schmidt variation in the front head position, show that simulations with double mass diffusivity reach a greater distance than simulations with Schmidt unitary after the flow gets in the deceleration phase and keeps this situation for the rest of the computational time. For suspended mass, it is observed that the fine particles are deposited more quickly by increasing the Schmidt number. Also, it is observed that an increase in the Schmidt number caused a smoothness in the peaks present in the deposit profile. For the temporal evolution of the energy budget, the results show that the principal mechanism for energy dissipation is related to turbulent dissipation, which also increases with the Schmidt number.*

***Keywords:*** *Bi-disperse current, particle-laden gravity current, direct numerical simulation, large eddy simulation, deposition of particles*

## 1. INTRODUCTION

Density current, or gravity current, is a type of flow where the motion of one fluid through another is caused by a density difference between them. When the main gradient is in the horizontal direction, one fluid propagates horizontally through the other. The variation of density could be caused by a difference in temperature, salinity, or by particles in suspension. This kind of flow occurs in many natural situations as well as created by humankind. Some examples are thunderstorm outflow, sea-breeze fronts, airborne snow, sandstorm, powder snow avalanches, and pyroclastic flows. In the ocean, these flows are driven by salinity and temperature inhomogeneities, or like in turbidity currents whose density gradients derive from suspended mud or silt. Density currents own important applications in aircraft safety, entomology, pest control, and spreading pollutants in rivers, lakes, and the atmosphere. In the industry, this kind of flow could be observed in the manufacturing process of sheet glass. For engineering, gravity currents are extremely dangerous since they can destroy seafloor equipment like pipes and cables (Ellison and Turner, 1959; Simpson, 1982).

Turbidity currents are particle-laden gravity-driven underflows in which the particles are largely or wholly suspended by fluid turbulence. The turbulence is typically generated by the forward motion of the current along the lower boundary of the domain, the motion in turn driven by the action of gravity on the difference between the particle-fluid mixture and the ambient fluid. Such flows are considered nonconservative due that they may exchange particles with a loose lower boundary by deposition or suspension, and may exchange fluid with the ambient by entrainment or detrainment. Turbidity currents are important agents of sediment transport into subaqueous environments such as deep lakes and oceans. This kind of flow along with submarine landslides are the principal mechanism by which sediment is transported from shallower to deeper water (Meiburg and Kneller, 2010). In the oceans, submarine flows can generate deposits several thousands of kilometers from their source (Talling *et al.*, 2007). The industry of oil and gas has a great interest to understand this kind of flow, because deposits of sand formed by turbidity currents have a high potential to become hydrocarbon deposits.

There are many ways to study the behavior of density current. One approach is through the mathematical modeling of

the governing equations which rule the dynamic of the flow. Another way is through physical experiments which consist in reproducing this phenomenon on a reduced scale, this could be done by filling a tank with water and creating a flow by releasing another fluid of a different density into the tank. Some examples of this kind of approach are Middleton (1966), Simpson (1972), Huppert (1982) and Gladstone *et al.* (1998). Also, the behavior of gravity current can be understood by a numerical approach where the governing equations are solved by a numerical scheme. Some works that utilize this methodology are Kubo (2004), Necker *et al.* (2005), Cantero *et al.* (2007), Espath *et al.* (2014), Nasr-Azadani *et al.* (2013), Nasr-Azadani *et al.* (2016), Francisco *et al.* (2017), and Frantz *et al.* (2021).

One of the most important parameters in the simulation of a density current is the Schmidt number (*Sc*). This dimensionless parameter is defined as the ratio of kinematic viscosity and the mass diffusivity, and it is related to how the heavy and light fluids can mix being a important factor in determining the structure and the dynamics of the current. At the macroscale, the mixing is caused by interfacial instabilities, while at the molecular level is controlled by the diffusivity of the agent responsible for density difference. In gases and liquids, thermal and concentration diffusivities show wide variation. For example, the Schmidt number for thermal diffusivity in the air is around 0.7, while in water it is about 7.0. In contrast, the Schmidt number for salt and several other solvents in water is at the order of $O\left(10^2\right)$. For immiscible fluids, like oil and water, the Schmidt number tends to have very high values with mixing occurring only at macro-scale through interfacial instability and turbulence (Bonometti and Balachandar, 2008). Nevertheless, most of the studies in numerical simulation only consider the value 1 for the Schmidt number, even though this parameter can reach values of greater order.

Necker *et al.* (2005) tested the influence of Schmidt number in their simulations. They got that the flow is independent for Schmidt number not much smaller than one. Bonometti and Balachandar (2008) analyzed the effect of Schmidt number for the structure and dynamic of density current. Their results show that there is a weakly influence of this parameter for simulations with Reynolds number greater than $O(10^4)$. On the other hand for low and moderate Reynolds density currents are dependant on Schmidt as the structure of the mixing region and front head velocities are modified by diffusion effects. Marshall *et al.* (2021) performed tree-dimensional simulations to investigate the effect of Reynolds and Schmidt number in the structure and dynamic of density current. They find that some features of the flow are independent of the Schmidt number, like the head front velocity, otherwise the appearance of lobe-and-cleft structures in the head show great influence of Schmidt number even with increasing of Reynolds number. Other features, like the thickness of the current, the Schmidt number lost relevance by increasing the Reynolds number.

This study uses a numerical approach to understand the behavior of particle-laden gravity current. The goal of this research is to investigate the influence of the Schmidt number on the dynamic of the flow, so direct numerical simulations (*DNS*) and implicit large eddy simulations (*LES*) of bi-disperse particle-laden gravity currents in a lock-release configuration (see Fig. 1) are performed. Numerical experiments of the same initial concentration of coarse and fine particles fractions are performed for unique and different values of Schmidt number with the same Reynolds number of 5000. The in-house code *Xcompact3d* is used to solve the incompressible Navier-Stokes equations by a numerical approach. To quantify the study, some features of the flow are calculated like the front head position, suspended mass, and deposit profile. Also, the complete temporal evolution of the energy budget of the current is calculated. For validation of the numerical scheme utilized in this study the results of the simulations are compared with physical experiments of Gladstone *et al.* (1998).

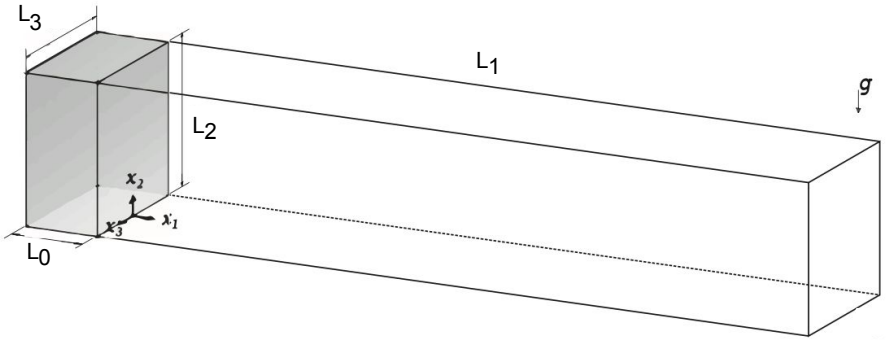


Figure 1. Schematic view of initial condition of lock-release configuration. The lock (filled region) is the place where the mixture is confined at the start of the simulation $(t = 0)$. The calculation domain has length $L_1$, height $L_2$, and width $L_3$. $L_0$ is the length of the lock region. Adapted from Francisco *et al.* (2017).

## 2. METHODOLOGY

In this section, the governing equations, the flow configuration as well as the treatment for the data post-processing will be described.

### 2.1 Governing equations and boundary conditions

This numerical study uses the lock-release configuration in his approach. In the initial state of this configuration $(t = 0)$ the mixing is restricted to a subarea of the domain, called lock, isolate from the rest of the domain by a gate. The experiment begins by removing the gate and the mixing start to flow. From this moment two mechanisms yield the flow motion: (i) the first one is caused by the transformation of potential energy into kinetic energy, leading to advective motion, and (ii) the other is the diffusive motion that is generated by the potential density difference between heavy and light fluid.

To evaluate the flow motion the incompressible Navier-Stokes equations and scalar transport equation under the Boussinesq approximation are solved using a numerical approach. The height of domain $L_2$ is used with characteristic length scale $\tilde{h}$ (the symbol ˜ is used to denote dimensional quantities while the others are dimensionless), $\tilde{h} = L_2$, the buoyancy velocity $\tilde{u}_b$ is defined as

$$\tilde{u}_b = \sqrt{\tilde{g}'\tilde{h}}, \tag{1}$$

where $\tilde{g}'$ is the reduced gravitational acceleration given by

$$\tilde{g}' = \frac{\tilde{g}\left(\tilde{\rho}_p - \tilde{\rho}_0\right) c_{t_0}}{\tilde{\rho}_0}, \tag{2}$$

where $\tilde{g}$ is the gravitational acceleration, $\tilde{\rho}_p$ is the mixing density, $\tilde{\rho}_0$ is the density of ambient fluid, and $c_{t_0}$ is the initial total concentration inside the lock.

The Reynolds and Schmidt number are defined as

$$Re = \frac{\tilde{u}_b\tilde{h}}{\tilde{\nu}}, \tag{3}$$

$$Sc_l = \frac{\tilde{\nu}}{\tilde{k}_l} \qquad l = 1, ..., N, \tag{4}$$

where $\tilde{\nu}$ denotes the kinematic viscosity, $Sc_l$ and $\tilde{k}_l$ are respectively the Schmidt number and the mass diffusivity coefficient for each particle fraction $l$. $N$ is the total number of particle fractions in the current, being each fraction characterized by a different diameter. In this study, all the simulations performed are bi-disperse ($N = 2$).

In the dimensionless form, the Navier-Stokes equations and scalar transport equation can be written as

$$\frac{\partial u_i}{\partial x_i} = 0, \tag{5}$$

$$\frac{\partial u_i}{\partial t} + u_j\frac{\partial u_i}{\partial x_j} = -\frac{\partial p}{\partial x_i} + \frac{1}{Re}\frac{\partial^2 u_i}{\partial x_j\partial x_j} + c_t e_i^g, \tag{6}$$

$$\frac{\partial c_l}{\partial t} + \left(u_j + u_l^s e_j^g\right)\frac{\partial c_l}{\partial x_j} = \frac{1}{Sc_l Re}\frac{\partial^2 c_l}{\partial x_j\partial x_j} \qquad l = 1, ..., N, \tag{7}$$

where $u_i$ and $p$ are respectively the velocity and pressure field, $i$ and $j$ are indexes for each spatial coordinate. $c_l$ and $u_l^s$ are respectively the concentration field and the settling velocity for each particle fraction $l$. $e_j^g = (0, -1, 0)$ is the unitary vector acting in the direction of the gravitational acceleration.

The total concentration field $c_t$ could be calculated by the sum of concentration for each particle fraction

$$c_t = \sum_{l=1}^{N} c_l \qquad l = 1, ..., N. \tag{8}$$

At start of the simulation $(t = 0)$ the value of $c_t$ is 1 in lock region and 0 for the rest of the domain.

As was previously discussed, the Schmidt number could be very high and computationally expensive to simulate. To overcome this problem, an estimation based on the diffusivity coefficient for each particle is used, considering the Einstein-Stokes equation (Bird *et al.*, 2004),

$$\tilde{k}_l = \frac{\tilde{k}_B\tilde{T}}{6\pi\tilde{\mu}\tilde{r}_l}, \tag{9}$$

where $\tilde{k}_B$ is the Boltzmann constant, $\tilde{T}$ is the absolute temperature, $\tilde{\mu}$ is the dynamic viscosity coefficient, and $\tilde{r}_l$ is the radius of each particle fraction $l$.

Applying the ratio between the Schmidt number for the two-particle fraction and considering the Eq. 9 the following relation arrives

$$\frac{Sc_1}{Sc_2} = \frac{\tilde{k}_2}{\tilde{k}_1} = \frac{\tilde{r}_1}{\tilde{r}_2}. \tag{10}$$

Considering typical values of $69\mu m$ and $25\mu m$ for coarse and fine particle fraction, which are the same values of the particles in the experiments of Gladstone *et al.* (1998), and apply the Eq. 10 it is calculated the value $\approx 3$ for the ratio $Sc_1/Sc_2$. In this study, this ratio was used in the simulations with different values of mass diffusivity.

A Cartesian mesh with $n_1 \times n_2 \times n_3$ grid points is used in a domain of size $L_1 \times L_2 \times L_3$. To reproduce the effect of removing the gate at the beginning of the experiment a white noise with $1\%$ of the initial potential energy is used in the interface between the lock and the flesh fluid.

For the velocity field, a no-slip boundary condition is applied at the bottom and top of the domain ($x_2 = 0$ and $x_2 = L_2$), and free-slip for the rest of the domain. For the scalar field the Neumann condition is used for the bottom and top of the domain ($x_2 = 0$ and $x_2 = L_2$), and no-flux for the other boundaries in the domain. To take into account the particles deposition in the vertical direction at the bottom of the domain, the following outflow boundary condition is used

$$\frac{\partial c_l}{\partial t} + u_l^s e_2^g \frac{\partial c_l}{\partial x_2} = 0 \tag{11}$$

at $L_2$.

The Equation 11 allows mimicking the process of sediment leaving the computational domain when the particles touch the bottom wall. In the configuration utilized the process of erosion and resuspension are not implemented.

The DNS and LES approaches are used in this study to solve the Navier-Stokes equations and the scalar transport equation. The mean difference between those two numerical schemes is the strategy to deal with the small scales of the flow. In the DNS approach, all scales of the flow can be represented in the mesh grid, whereas in LES the small scales are neglected by a low-pass filter Lesieur *et al.* (2005). In the DNS scheme the mesh size $\Delta x$ is close to Kolmogorov scale $\eta$, $\Delta x \approx \eta$, which is enough to ensure the accuracy for the model, even though involves more computational time to solve the flow equations. On the other hand, for the LES approach the mesh size is close to the filter size $\Delta$, $\Delta x \approx \Delta$, which allows the scheme to save computational time, but requires the use of a subgrid-scale model to reproduce the dissipation caused by the small scales (Dairay *et al.*, 2017). The LES simulations performed in this study use a method based on the spectral vanishing viscosity, which consists in add a viscosity dissipation in the calculation of the second derivative of the diffusion term (Lamballais *et al.*, 2011; Frantz *et al.*, 2021).

### 2.2 Post-processing

In the post-processing of the data, some features of the flow are calculated, like the front head position, the suspended mass, and the height of the deposit.

To determine the front head position $x_f$ the method used in Cantero *et al.* (2007) is applied in this study. This framework consists in integrating the scalar field in the directions $x_2$ and $x_3$ to get the average concentration in direction $x_1$, this can be expressed in the equation

$$\overline{c}_t\left(x_1, t\right) = \frac{1}{L_2 L_3} \int_0^{L_2} \int_0^{L_3} c_t \, dx_2 dx_3, \tag{12}$$

where $\overline{c}_t$ is the total average concentration in function of $x_1$. With this definition, the front head position could be computed as the most forward position where the average concentration reaches a threshold value. In this study, it is used the value of $0.1\%$ of the total concentration field.

Farenzena and Silvestrini (2021) analyze different methods and strategies to minimize uncertainties in the temporal evolution of the front velocity. They also propose a new approach for front head determination based on a moving frame of reference, which avoid the use of an arbitrary iso-value. They found that a more accurate measurement of the front head position can be reached by the interpolation of the front head acquisition method or by using the moving frame of reference proposed in the article. This study uses the strategy of interpolation of the scalar field to minimize the uncertainties in the calculation of the front head position.

The temporal evolution of suspended mass is performed as integral of the scalar field in the computational domain $\Omega$ defined as

$$m_{p_l}\left(t\right) = \int_\Omega c_l d\Omega \qquad l = 1, ..., N, \tag{13}$$

where $m_{p_l}$ is the suspended mass for each particle fraction $l$.

The Equation 11 allows the code mimics the process of sediments leaving the domain at touch the bottom wall. It is possible to calculate the height of the deposit generated from the process of sedimentation by the time integration of the scalar field at the bottom of the domain. The height of the deposit for each particle fraction in the function of the time is defined as

$$D_l\left(x_1,t\right)=\int_0^t < c_{w_l(x_1,\tau)} >_{x_3} u_l^s d\tau \qquad l=1,...,N, \tag{14}$$

where $D_l$ is the average height of the deposit in the function of $x_1$ and the time, the operator $< . >$ denotes the spanwise averaging. The profile of total mass deposited is expressed by

$$D_t\left(x_1,t\right)=\sum_{i=1}^{N} D_l\left(x_1,t\right) \qquad l=1,...,N, \tag{15}$$

where $D_t$ is the total average height profile.

### 2.3 Energy budget

In essence, any gravity-driven flow can be understood as a conversion of potential energy into kinetic energy which subsequently is dissipated into heat by viscous friction (Necker *et al.*, 2005). The main difference between density-driven gravity currents and particle-laden gravity currents is that dissipation occurs not only at the macroscopic scale with the strain rate, but also at the microscale around each particle (Espath *et al.*, 2014).

In Winters *et al.* (1995) is proposed a framework to calculate the energy budget of the flow. Necker *et al.* (2005) use the approach of the previous study, but they assume some simplifications like neglecting the effects of diffusion in the concentration field has on the potential energy. In this study, the step-by-step proposed in Espath *et al.* (2014) is used, in their approach the energy budget of the flow is computed without any assumptions over the dissipation terms.

The energy budget for an incompressible flow with particle concentration in the dilute suspension approach can be extracted from the governing equation and scalar transport equation. An expression for time variation of total mechanical energy can be evaluated by

$$\frac{d\left(k+E_{p_t}\right)}{dt}=-\int_\Omega \frac{2}{Re}s_{ij}s_{ij}d\Omega+\sum_{l=1}^{N}\left[\int_\Omega x_2\frac{1}{Sc_l Re}\frac{\partial^2 c_l}{\partial x_2 \partial x_2}d\Omega+\int_\Omega x_2 u_l^s\frac{\partial c_l}{\partial x_2}d\Omega\right]=-\epsilon_d-\epsilon_{s_t}, \tag{16}$$

where $k$ and $E_{p_t}$ are respectively the kinetic and the total potential energy. $s_{ij}=\left(\frac{\partial u_i}{\partial x_j}+\frac{\partial u_j}{\partial x_i}\right)$ is the strain rate tensor. The term $\epsilon_d$ is the dissipation rate related to turbulence, whereas $\epsilon_{s_t}$ is the total dissipation rate associated with mass diffusion and mass loss due to sedimentation.

Integrating the terms $\epsilon_d$ and $\epsilon_{s_t}$ over the time it gets the equations

$$E_d\left(t\right)=\int_0^t \epsilon_d\left(\tau\right)d\tau, \tag{17}$$

$$E_{s_t}\left(t\right)=\sum_{l=1}^{N}E_{s_l}\left(t\right)=\sum_{i=1}^{N}\left[\int_0^t \epsilon_{s_l}\left(\tau\right)d\tau\right], \tag{18}$$

where $E_d$ is the total energy dissipated for the convective motion. $E_{s_l}$ and $\epsilon_{s_t}$ are respectively the temporal integration and instantaneous microscopic dissipation for each particle fraction. $E_{s_t}$ is the total energy loss by microscopic effects.

Finally, the complete energy budget equation is given by

$$k+E_{p_t}+E_d+E_{s_t}=E_{t_0}=k_0+E_{p_0}, \tag{19}$$

where $E_{t_0}$, $k_0$, and $E_{p_0}$ are respectively the total energy mechanics, kinetic energy, and potential energy at beginning of the simulation $(t=0)$.

### 2.4 Software

To solve the Navier-Stokes equations for incompressible fluids and scalar transport equation the code *Xcompact3d*, available at https://github.com/xcompact3d/Incompact3d, is employed. *Xcompact3d* is a software developer in *FORTRAN 90* able to solve the equations for incompressible flows for both DNS and LES approaches. The code uses a compact scheme of sixth-order finite difference for spatial differentiation (Lele, 1992) and a third-order Adam-Bashford for time integration. For more information about compact schemes and the parallel strategy used for *Xcompact3d* it is recommended reading the works of Laizet and Lamballais (2009) and Laizet and Li (2010).

### 2.5 Global parameters

DNS and LES of bi-disperse particle-laden gravity currents in lock-release configuration are performed, in Tab. 1 the global parameters of the four simulations analyzed in this study can be viewed. Three of them are performed with the LES approach for unique and different values of Schmidt number, a one case using the DNS approach is performed to be used as a benchmark. The Reynolds number of 5000 is used in all simulations. The domain is dimensionless using the definition of the characteristic length scale present at beginning of this section for the experiments of Gladstone *et al.* (1998). The dimensionless domain size use in all simulations are $L_1 = 17$, $L_2 = 1$, and $L_3 = 0.5$. $L_0 = 0.5$ is the length of lock region at beginning of the simulation ($t = 0$). For all cases, it is used the time step of $\Delta t = 5 \times 10^{-4}$ and the interval of 1 dimensionless time is used as the frequency for saving the data. All the simulations are stopped at the dimensionless time of $t = 90$. The settling velocity for coarse and fine particle fraction are respectively $u_1^s = 0.03$ and $u_2^s = 0.004$.

The terms $\nu/\nu_0$ and $k/k_0$ in Table 1 are the numerical dissipation in the numerical scheme for respective velocity and scalar field to deal with dissipation generated by the small scales (Dairay *et al.*, 2017; Sun and Domaradzki, 2018). Different values of dissipation for velocity and scalar field are used to increase the Schmidt number without a great increase in the mesh grid size.

All the simulations are done in the Laboratório de Alto Desempenho (LAD) of PUCRS. The parallel processing is done using the MPI protocol in 4 machines with 12 cores each, in total 96 nodes are used. The machines have Intel Xeon E5-2620 and E5645 processors, depending on the machine allocation the cloak could vary between 2.0 GHz and 2.4 GHz, and 24 to 32 GB of RAM. The time needed to perform each simulation varied between some hours to one week.

Table 1. Global parameters. In each column there is: (i) the simulation label; (ii) the number of points in the coordinates $x_1$, $x_2$, and $x_3$; (iii) the Schmidt number for coarse and fine particle fraction; (iv) the numerical dissipation for flow field; (v) and the numerical dissipation for the concentration field.

| Simulation | $(n_{x_1}, n_{x_2}, n_{x_3})$ | $Sc_1/Sc_2$ | $\nu/\nu_0$ | $k/k_0$ |
|---|---|---|---|---|
| $DNS1$ | $(2023, 239, 61)$ | $(1, 1)$ | 4 | 4 |
| $LES1$ | $(727, 85, 21)$ | $(1, 1)$ | 12 | 12 |
| $LES2$ | $(727, 85, 21)$ | $(3, 1)$ | 12 | 16 |
| $LES3$ | $(945, 127, 27)$ | $(9, 3)$ | 12 | 24 |

## 3. RESULTS

In this section, the results of the simulations in Tab. 1 are discussed.

### 3.1 Visualization

In Figure 2 can be seen the snapshot of the scalar field for coarse and fine concentration particles at time $t = 10$. Notice that there is no differentiation on the front head position for coarse and fine particle fractions. It is also possible to observe the formation of some structures in the flow like Kelvin-Helmholtz vortexes behind the head of the current. For the variation of Schmidt, it is observed the formation of more complex structures as it increases the mass diffusivity, which shows that some features of the flow could not be observed if this parameter is neglected. Comparing the simulations *DNS1* and *LES1* - both simulations with the same Reynolds number and Schmidt number, but with one using the DNS approach and the other LES - there are few differences between both, being the mean difference between the two fields around $3\%$.

### 3.2 Temporal evolution of front head position

In Figure 3 the temporal evolution of the front head position of the current is plotted, where the initial position is defined as gate location. The results are compared with the experiments of Gladstone *et al.* (1998) and show a good agreement until $t \approx 10$, when the simulations stayed behind in comparison with the physical case, which is expected due to the high Reynolds ($Re \approx 70000$) number of the reference case. Analyzing all cases notice that until $t \approx 10$ the flow moves with constant velocity, proportional to $\sim t^1$, and there is no perceptible difference among the simulations. After this time the flow enters a deceleration phase and after $t \approx 20$ the difference among the front head of the simulations starts to show.

For the effect of Schmidt number it is observed a great difference between the simulations with different mass diffusivity (*LES2* and *LES3*) and the simulations with unique Schmidt number (*DNS1* and *LES1*). The front head position of simulations with double mass diffusivity remains ahead in comparison with simulations with unitary Schmidt number from the time $t = 20$ until the end of the computational time. This suggests that considering double mass diffusivity will

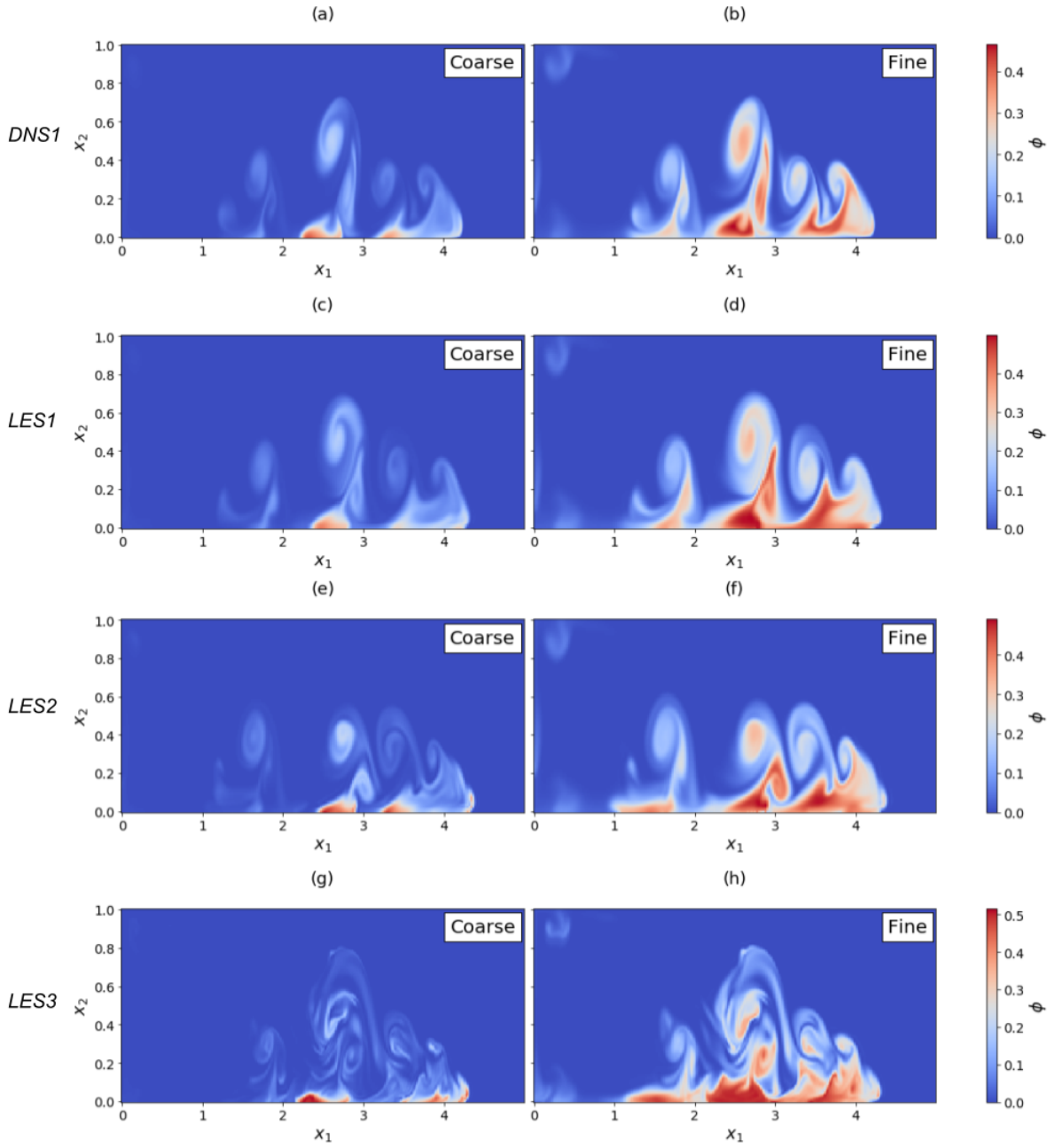


Figure 2. Snapshot of the scalar field for coarse and fine concentration particles fraction at time $t = 10$ and position $x_3 = 0.25$.

affect the temporal evolution of the flow front head. Although increasing the mass diffusivity does not generate a great difference between simulations *LES2* and *LES3*, which indicates that increasing the Schmidt number for this interval did not have a great impact. Comparing the simulations *DNS1* and *LES1* shows that there are weak differences in the time evolution of front head position for these two simulations, with a mean difference of $7\%$. This indicates that the LES approach can reproduce with good approximation the result of a simulation using the DNS approach, even with a number of points around $4\%$ of the total number of points from a DNS.

### 3.3 Suspended mass and deposit mean profile

In Figure 4 can be seen the temporal evolution of suspended mass for coarse particle fraction $m_{p_1}$, fine particle fraction $m_{p_2}$, and total suspended mass fraction $m_{p_t}$. All curves are normalized by the total of suspended mass at the start of the simulation $(t = 0)$.

At the beginning of the simulation can be observed that the initial concentration of coarse and fine particles fractions is equal to the initial concentration at the lock. After the mixture starts to flow the coarse particle fraction, Fig 4.a, suffers

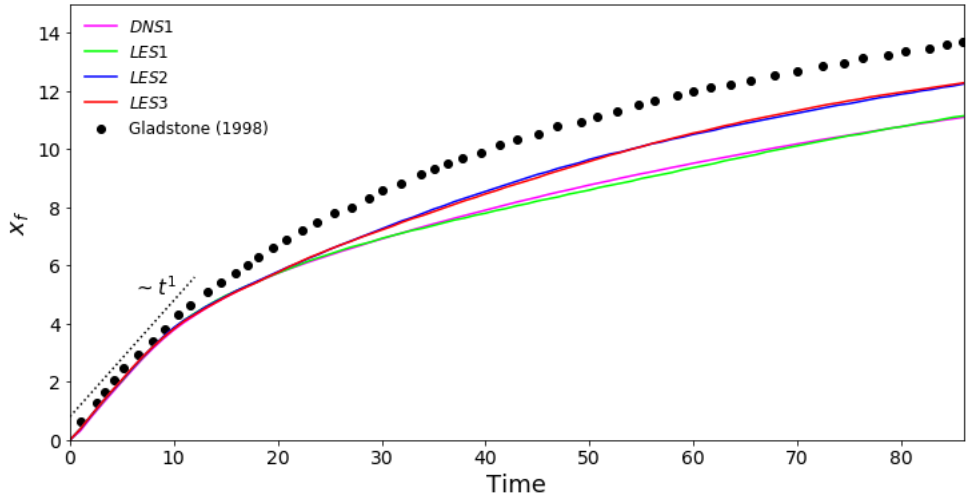


Figure 3. Temporal evolution of the front head position for the four simulations compared with the reference experiment of Gladstone *et al.* (1998). It is considered the gate location as $x_1 = 0$.

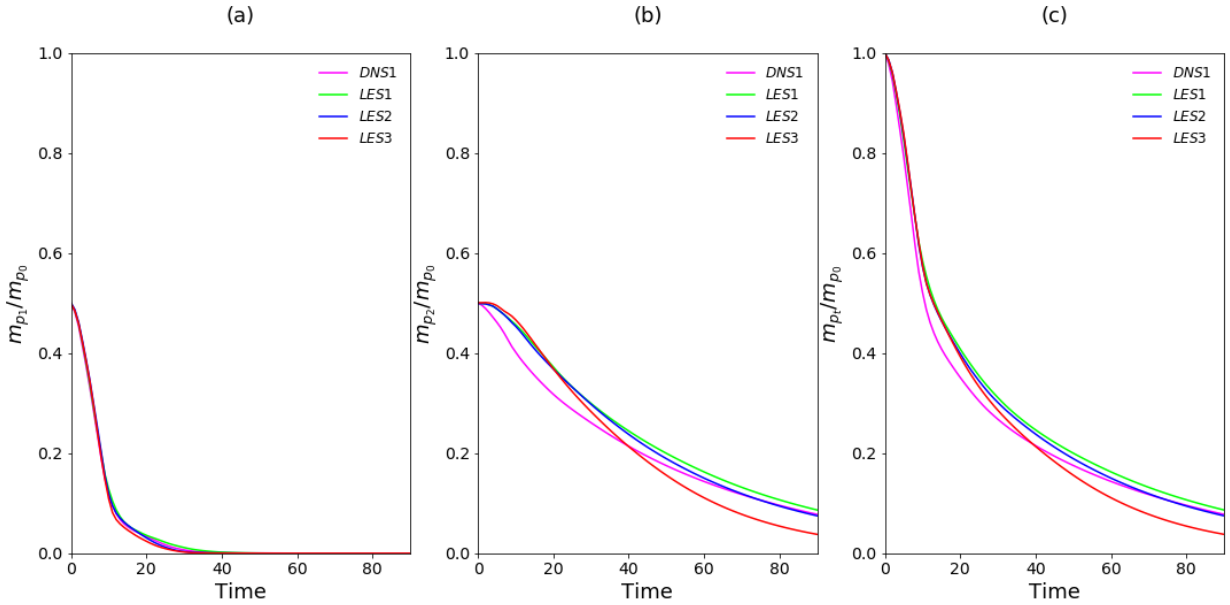


Figure 4. Temporal evolution of suspended mass for (a) fine particles fraction, (b) coarse particles fraction, and (c) total of suspended mass (a+b). All curves are normalized by total of suspended mass at the start of the simulation $(t = 0)$.

a quickly decreasing with less than $26\%$ of the initial mass for the coarse particle fraction still suspended at $t = 10$, while in $t = 20$ there is less than $8\%$ of the initial material, and for $t = 40$ this reaches less than $1\%$. There are weak differences among the simulations for the suspended mass of coarse particle fraction.

Analyzing the suspended mass for fine particle fraction, Fig. 4.b, notice that there is also a decrease after the beginning of the flow, although it is less impactful than the one suffered for coarse particle fraction. At $t = 10$ the simulation which has the great decrease is *DNS1*, with $80\%$ of the initial mass still suspended, for the other simulations, this value fluctuates between $91\%$ and $93\%$. In $t = 20$, around $63\%$ of the initial quantity of particle fraction keeps suspended for simulation *DNS1* e between $73\%$ and $75\%$ for the others, although this decrease is smaller than what happened for coarse particle fraction. At $t = 40$ there is less than $1\%$ of the total coarse particle fraction suspended, but more than $43\%$ of the total fine particle fraction is kept suspended. At the end of the computational time, $(t = 90)$, $7\%$ of the fine particle fraction remains suspended. This aspect is a characteristic of the particle fine fraction because the fact that they stay suspended for more time makes them the principal mechanism to keep the density gradient, allowing the flow to reach greater distances. This has already been observed experimentally by Gladstone *et al.* (1998) and computationally by Francisco *et al.* (2017). Looking at the effect of the Schmidt number it is noticed there is a decrease in the particle fraction suspended at end of the simulation as it increases the Schmidt number. In the end of the computational time $(t = 90)$ the simulations *DNS1*, *LES1*, *LES2*, and *LES3* posses respectively $15.16\%$, $17.30\%$, $14.98\%$, and $7.58\%$ of the initial mass still suspended.

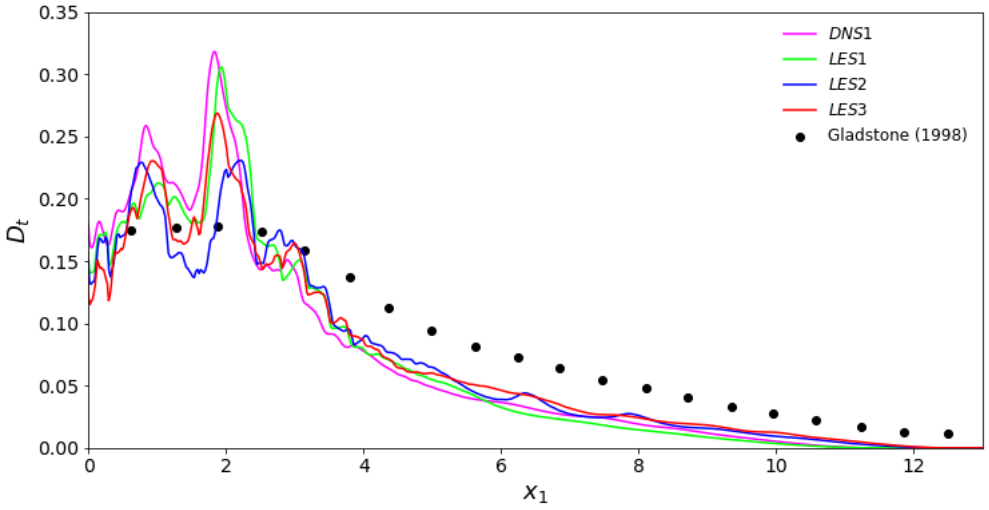


Figure 5. Final deposit profile for the four simulations compared with the reference experiment of Gladstone *et al.* (1998). All curves are normalized by the volume of deposit at end of the simulation, $t = 90$. The initial position $x_1 = 0$ was chosen as *gate* position.

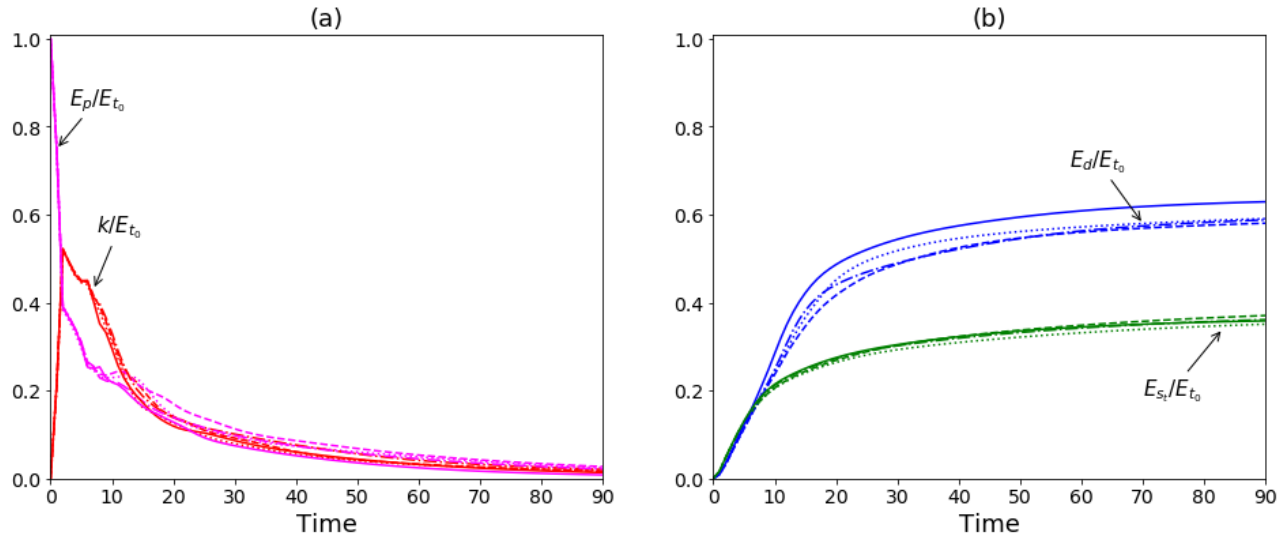


Figure 6. Temporal evolution of energy budget for the four simulations. Dotted curves correspond to simulation *DNS1*, dashed lines correspond to simulation *LES1*, dashdot curves correspond to simulation *LES2*, and solid lines correspond to simulation *LES3*.

In Figure 5 the average profiles of deposit height for the four simulations are plotted compared with the reference experiment of Gladstone *et al.* (1998). All curves are normalized by the volume of deposit at end of the simulation ($t = 90$). Comparing the deposit profiles with the reference it is observed a good agreement. The peaks that occurred for $x_1 < 2$, are probably related to the Kelvin-Helmholtz vortex since those vortexes can enhance the particle deposition when passing near the bottom. It is observed that most of the deposit was formed close to the gate, which is common for this kind of configuration. Analyzing the effect of mass diffusivity notice that there is a tendency to smooth the peaks with the Schmidt number increase. Comparing the simulations *DNS1* with *LES1* there is a mean difference of $0.75\%$. This indicates that the LES approach can reproduce a deposit profile similar to the one generated by a DNS simulation.

### 3.4 Energy budget

The temporal evolution of budget energy flow for the four simulations is plotted in Fig. 6. All curves are normalized by total energy at the beginning of the simulation $E_{t_0}$ $(t = 0)$.

Observing the curves for potential $E_p/E_{t_0}$ and kinetic energy $K/E_{t_0}$, Fig. 6.a, at $t = 0$ the potential energy is maximum while the kinetic energy is minimum. After the mixture starts to flow the potential energy begins to suffer a great decrease, whereas the kinetic energy increases quickly, reaching its peak at $t = 2$ with around $52\%$ of total initial

energy. Although, after getting this peak the kinetic energy suffers a decrease due to the dissipation effects which gain more importance in the energy budget. At the end of simulation ($t = 90$) the potential energy for simulations *DNS1*, *LES1*, *LES2*, and *LES3* are respectively $2.45\%$, $2.73\%$, $2.18\%$, and $0.85\%$, and for the kinetic energy are $1.82\%$, $1.7\%$, $2.07\%$, and $1.38\%$, respectively.

Analyzing the curves for turbulence energy dissipation $E_d/E_{t_0}$ and for microscale dissipation $E_{s_t}/E_{t_0}$, Fig. 6.b, it is noticed that the term $E_d/E_{t_0}$ have more importance in the dissipation's effects. At $t = 90$ the value of the dissipation due to turbulence for simulations *DNS1*, *LES1*, *LES2*, and *LES3* are respectively $59.08\%$, $58.06\%$, $58.81\%$, and $62.93\%$ of total initial energy, while for microscales effects are respectively $35.11\%$, $37.07\%$, $36.14\%$, and $35.87\%$. Looking at the influence of the Schmidt number, it is observed that by increasing this parameter the term $E_d$ became more relevant in the budget energy, especially when there is an increase in the Schmidt number between simulations *LES2* to *LES3*.

## 4. CONCLUSION

Simulations of bi-disperse particle-laden gravity currents are performed in the lock-release configuration using DNS and LES approach. The goal of this study is to analyze the effect of different Schmidt numbers on the flow dynamics and the formation of his deposits. So simulations with unique and different mass diffusivity are performed with the same Reynolds number of 5000. To quantify the study some features of the current are calculated like the front head position, the suspended mass, and the average height profile of the deposit. Also, it is computed the temporal evolution of the energy budget. The results are in good agreement with the experimental results of Gladstone *et al.* (1998). For the front head position, the effect of using different values for the two-particle fractions has a great impact on the temporal evolution of the flow, with the flows with double mass diffusivity reaching greater distance compared with the flows with unique Schmidt number at end of the simulation. Although, increasing the Schmidt number does not cause a great difference between the simulations *LES2* and *LES3*. For the suspended mass the quantity of coarse particle fraction is almost deposited at $t = 40$, with less than $1\%$ of the initial quantity of coarse particle fraction still suspended, in the other hand the fine particle fraction keeps a significant quantity of the original material still suspended at end of the simulation, between $7\%$ and $15\%$. Analyzing the effect of the Schmidt number in the suspended mass it is noticed that increasing this parameter will be more fine particles fraction deposited at end of the simulation. The average deposit profile shows good agreement with the experimental results, it is observed that increasing the Schmidt number more smooth the peaks of the deposit will be. For the energy budget, it is observed that the dissipation relate to turbulence is the principal mechanism of energy loss and gains more relevance as it increases the Schmidt number.

## 5. ACKNOWLEDGEMENTS

This study was achieved in cooperation with Hewlett-Packard Brasil Ltda. using incentives of Brazilian Informatics Law (Law nº 8.2.48 of 1991). This study have the support of Laboratório de Alto Desempenho (LAD) of PUCRS.

## 6. REFERENCES

Bird, R.B., Stewart, W.E. and Lightfoot, E.N., 2004. *Transpot phenomena 2 edition.*

Bonometti, T. and Balachandar, S., 2008. "Effect of schmidt number on the structure and propagation of density currents". *Theoretical and Computational Fluid Dynamics*, Vol. 22, pp. 341–361.

Cantero, M.I., Lee, J.R., Balachandar, S. and Garcia, M.H., 2007. *On the front velocity of gravity currents*, Vol. 586. ISBN 0022112007005. doi:10.1017/S0022112007005769.

Dairay, T., Lamballais, E., Laizet, S. and Vassilicos, J.C., 2017. "Numerical dissipation vs. subgrid-scale modelling for large eddy simulation". *Journal of Computational Physics*, Vol. 337, pp. 252–274.

Ellison, T.H. and Turner, J.S., 1959. "Turbulent entrainment in stratified flows". *Fluid Mechanics*, Vol. 6, pp. 423–448. URL `https://doi.org/10.1017/S0022112059000738`.

Espath, L.F.R., Pinto, L.C., Laizet, S. and Silvestrini, J.H., 2014. "Two- and three-dimensional direct numerical simulation of particle-laden gravity currents". *Computers & Geosciences*, Vol. 63, pp. 9–16.

Farenzena, B.A. and Silvestrini, J.H., 2021. "Density currents front velocity uncertainty". *Computer & Fluids*.

Francisco, E.P., Espath, L.F.R. and Silvestrini, J.H., 2017. "Direct numerical simulation of bi-disperse particle-laden gravity currents in the channel configuration". *Applied Mathematical Modelling*, Vol. 49, pp. 739–752.

Frantz, R.A.S., Deskos, G., Laizet, S. and Silvestrini, J.H., 2021. "High-fidelity simulations of gravity currents using a high-order finite-difference spectral vanishing viscosity approach". *Computers Fluids*. doi:104902. URL `https://doi.org/10.1016/j.compfluid.2021.104902`.

Gladstone, C., Phillips, J.C. and Sparks, R.S.J., 1998. "Experiments on bidisperse, constant-volume gravity currents: propagation and sediment deposition". *Sedimentology*, Vol. 45, pp. 833–843.

Huppert, H.E., 1982. "The propagation of two-dimensional and axisymmetric viscous gravity currents over a rigid horizontal surface". *Fluid Mechanics*, Vol. 121, pp. 43–58.

Kubo, Y., 2004. "Experimental and numerical study of topographic effects on deposition from two-dimensional, particle-driven density currents". *Sedimentary Geology*, Vol. 164, pp. 311–326.

Laizet, S. and Lamballais, E., 2009. "High-order compact schemes for incompressible flows: A simple and efficient method with quasi-spectral accuracy". *Journal of Computational Physics*, Vol. 228, No. 16, pp. 5989–6015. ISSN 10902716. doi:10.1016/j.jcp.2009.05.010. URL `http://dx.doi.org/10.1016/j.jcp.2009.05.010`.

Laizet, S. and Li, N., 2010. "Incompact3d: A powerful tool to tackle turbulence problems with up to $o(10^5)$ computational cores". *International Journal For Numerical Methods In Fluids*, Vol. 67, No. February, pp. 805–830. doi:10.1002/fld.

Lamballais, E., Fortuné, V. and Laizet, S., 2011. "Straightforward high-order numerical dissipation via the viscous term for direct and large eddy simulation". *Journal of Computational Physics*, Vol. 230, pp. 3270–3275.

Lele, S.K., 1992. "Compact finite difference schemes with spectral-like resolution". *Journal of Computational Physics*, Vol. 103, pp. 16–42.

Lesieur, M., Métais, O. and Comte, P., 2005. *Large-eddy simulations of turbulence*. Cambridge University Press.

Marshall, C., Dorell, R.M., Dutta, S., Keevil, G.M., Peakall, J. and Tobias, S.M., 2021. "The effect of schmidt number on gravity current flows: The formation of large-scale three-dimensional structures". *Physics of Fluids*, Vol. 33.

Meiburg, E. and Kneller, B., 2010. "Turbidity currents and their deposits". *Annual Review of Fluid Mechanics*, Vol. 42, pp. 135–156.

Middleton, G.V., 1966. "Experiments on density and turbidity currents i. motion of the head." *Canadian Journal of Earth Sciences*, Vol. 3, pp. 523–546.

Nasr-Azadani, M.M., Hall, B. and Meiburg, E., 2013. "Polydisperse turbidity currents propagating over complex topography: Comparison of experimental and depth-resolved simulation results". *Computers and Geosciences*, Vol. 53, pp. 141–153.

Nasr-Azadani, M.M., Meiburg, E. and Kneller, B., 2016. "Mixing dynamics of turbidity currents interacting with complex seafloor topography". *Environmental Fluid Mechanics*.

Necker, F., Härtel, C., Kleiser, L. and Meiburg, E., 2005. "Mixing and dissipation in particle-driven gravity currents". *Journal of Fluid Mechanics*, Vol. 545, pp. 339–372. ISSN 00221120. doi:10.1017/S0022112005006932.

Simpson, J.E., 1982. "Gravity Currents in the Laboratory, Atmosphere, and Ocean". *Annual Review of Fluid Mechanics*, Vol. 14, No. 1, pp. 213–234. ISSN 0066-4189. doi:10.1146/annurev.fl.14.010182.001241.

Simpson, J.E., 1972. "Effects of the lower boundary on the head of a gravity current". *Annual Review of Fluid Mechanics*, Vol. 53, pp. 759–768.

Sun, G. and Domaradzki, J.A., 2018. "Implicit les using adaptive filtering". *Journal of Computational Physics*, Vol. 359, pp. 380–408.

Talling, P.J., Wynn, R.B., Masson, D.G., Frenz, M., Cronin, B.T., Schiebel, R., Akhmetzhanov, A.M., Dallmeier-Tiessen, S., Benetti, S., Weaver, P.P., Georgiopoulou, A., Zühlsdorff, C. and Amy, L.A., 2007. "Onset of submarine debris flow deposition far from original giant landslide". *Nature*, Vol. 450, No. 7169, pp. 541–544. ISSN 14764687. doi:10.1038/nature06313.

Winters, K.B., Lombard, P.N., Riley, J.J. and D'Asaro, E.A., 1995. "Available potential energy and mixing in density-stratified fluids". *Journal of Fluid Mechanics*, Vol. 189, pp. 115–128.

## 7. RESPONSIBILITY NOTICE

The following text, properly adapted to the number of authors, must be included in the last section of the paper:
The authors are the only responsible for the printed material included in this paper.